

# Optimal Reference Tracking for Sampled-Data Control Systems

Enrico Bini<sup>1</sup>, Alessandro V. Papadopoulos<sup>2</sup>, Jacob Higgins<sup>3</sup>, Nicola Bezzo<sup>3</sup>

**Abstract**—It is a standard engineering practice to design feedback-based control to have a system follow a given trajectory. While the trajectory is continuous-time, the sequence of references is varied at discrete times as it is normally computed by digital systems.

In this work, we propose a method to determine the optimal discrete-time references to be applied over a time window of a given duration. The optimality criterion is the minimization of a weighted  $L^2$  norm between the achieved trajectory and a given target trajectory which is desired to be followed. The proposed method is then assessed over different simulation results, analyzing the design parameters' effects, and over a UAV use case. The code to reproduce the results is publicly available.

## I. INTRODUCTION

The majority of the engineering applications that surround us utilize feedback-based control mechanisms to track some reference signals by regulating control actions to achieve a desired system's behavior. For instance, this is the driving principle for most autonomous vehicle operations, including driverless cars and unmanned aerial vehicles, in which the main objective is to track some reference trajectory while minimizing time, energy, path deviation, or other user-defined costs. Other examples include cyber-physical system applications like tracking the temperature or other environmental states inside a building, deciding medication doses for patients in the health domain, managing traffic light signals in smart cities to minimize traffic congestion, and even regulating the production of goods in econometric supply-chain systems.

The desired trajectory to be followed is normally a continuous-time function since it represents a motion in the physical world. Instead, the reference given to the system so that the trajectory is followed is normally in discrete-time, since it is computed by digital systems. This paper introduces a new approach to computing the optimal discrete-time reference signal for a sampled-data control system to follow a desired continuous-time trajectory. The proposed approach is motivated by several control applications, where a fully designed control system is expected to track a trajectory in continuous time while having only discrete control time instants. For example, in industrial robotics applications, a waypoint controller may be required to follow a sequence of waypoints according to a timing law [1]. Another similar

problem is for the path planning of autonomous vehicles and mobile robots which typically requires waypoint tracking and static obstacle avoidance [2], [3].

The usage of sampled-data techniques for the control of linear systems is virtually ubiquitous, thanks to the flexibility given by the adoption of digital implementations of the control system [4], [5], [6]. However, even if sampled-data provide several advantages, the digital implementation sets limitations and constraints on the information available for feedback [7]. For example, the desired trajectory of the control system may be expressed in continuous time, but the reference signal can be set only at discrete time instants, leading to a potential detriment in tracking performance.

In the past, similar problems have been addressed by designing  $\mathcal{H}_2$  or  $\mathcal{H}_\infty$  hybrid control systems [8], [9], [10]. Most of these approaches focus on the solution of optimal and robust control problems via convex optimization problems whose constraints are expressed by LMIs [11], that ensure the optimal performance [12]. However, such approaches mostly focused on the optimal design of the digital controller. In this paper, we focus instead on the computation of the optimal reference signal in discrete-time given a desired trajectory of the system output, assuming that a control loop system has been designed.

The generation of a discrete-time reference signal can be thought of as similar to the problem of waypoint generation in robotics systems [13], [14], [15], [16], [17], [18]. Practical applications range from mobile robotics where waypoints are three-dimensional positions in space [19] to robotic manipulators that use waypoints defined within a more general state space [20]. In fact, the definition of waypoints implicitly defines a timing law of the reference trajectory. In the UAVs context, optimization-based techniques have been used to find the trajectory in cluttered environments while being robust to communication losses [21]. The contribution of this paper is inspired by this waypoint generation problem, but it abstracts from it, providing a more general solution. The Matlab implementation of the optimal reference computation is publicly available<sup>1</sup>.

The remainder of the paper is organized as follows. Section II presents preliminaries and the system model. Section III discusses the problem of trajectory tracking tackled in this paper, and Section IV presents the proposed solution. Section V shows simulation results, analyzing the effect of different design parameters. Finally, Section VI concludes the paper and sketches future work.

This work was supported by the Swedish Research Council (VR) with the PSI project (No. #2020-05094), by the Knowledge Foundation (KKS) with the FIESTA project (No. #20190034), by DARPA under Contract No. FA8750-18-C-0090, and by NSF under grants No. #1816591 and #1829004.

<sup>1</sup>E. Bini is with University of Turin, Italy

<sup>2</sup>A. V. Papadopoulos is with Mälardalen University, Sweden

<sup>3</sup>J. Higgins and N. Bezzo are with University of Virginia, USA

<sup>1</sup>[https://github.com/ebni/opt\\_ref\\_track](https://github.com/ebni/opt_ref_track)

## II. PRELIMINARIES AND SYSTEM MODEL

The notation used throughout this paper is as follows. For real vectors or matrices, the symbol  $\top$  refers to their transpose. The symbols  $\mathbb{R}$ ,  $\mathbb{R}_+$ , and  $\mathbb{N}$  denote the sets of real, non-negative real, and natural numbers, respectively. Vector variables are indicated with bold fonts, e.g.,  $\mathbf{x}$ . A function or trajectory  $f(t)$  that is sampled at time instants  $t = t_k$ , is denoted with  $f_k = f(t_k)$ , for  $k \in \mathbb{N}$ . The 2-norm of any vector  $\mathbf{x} \in \mathbb{R}^n$  is denoted by  $\|\mathbf{x}\| = \sqrt{\mathbf{x}^\top \mathbf{x}}$ . Finally, for any linear operator  $\mathcal{L}$ , we denote its null space (or *kernel*) by  $\ker \mathcal{L}$  that is  $\mathbf{x} \in \ker \mathcal{L} \Leftrightarrow \mathcal{L}\mathbf{x} = 0$ .

The system has an internal controller which is designed so that the output  $\mathbf{y}(t)$  follows a given reference  $\mathbf{r}(t)$  (represented by the block ‘‘Closed-loop Continuous-time Dynamics’’ in Figure 1). Section V-C shows the classic example of a PD-controlled double integrator. The internal continuous-time linear time-invariant dynamics of the system is given by

$$\begin{aligned} \dot{\mathbf{x}}(t) &= A\mathbf{x}(t) + B\mathbf{r}(t) \\ \mathbf{y}(t) &= C\mathbf{x}(t), \end{aligned} \quad (1)$$

with

- an internal *state*  $\mathbf{x}(\cdot) : \mathbb{R}_+ \mapsto \mathbb{R}^n$ ,
- a *reference* function  $\mathbf{r}(\cdot) : \mathbb{R}_+ \mapsto \mathbb{R}^m$ , to be followed, and
- the system *output*  $\mathbf{y}(\cdot) : \mathbb{R}_+ \mapsto \mathbb{R}^p$ .

We remark that despite  $\mathbf{r}(t)$  and  $\mathbf{y}(t)$  normally having images in the same space (that is  $m = p$ ), for generality, we keep them separate as our analysis can address the general case. We assume that the internal state  $\mathbf{x}(t)$  of the system is accessible. If this is not the case and if the system is observable, then an asymptotic observer can provide an accurate estimate of the internal state.

The internal state is sampled periodically, every period  $\tau$ . We denote the  $k$ -th sampling instant by  $t_k = k\tau$  and the state sampled at  $t_k$  by  $\mathbf{x}(t_k) = \mathbf{x}_k$ . The reference is held constant during every period, that is

$$\forall k, \forall t \in [k\tau, (k+1)\tau), \quad \mathbf{r}(t) = \mathbf{r}_k \quad (2)$$

with  $\mathbf{r}_k \in \mathbb{R}^m$  being the constant reference applied over the  $k$ -th interval.

To analyze the dynamics of (1) in the presence of a periodic piece-wise constant reference  $\mathbf{r}_k$ , we discretize it over the period  $\tau$ . For this purpose, we define

$$\Phi(t) = e^{At}, \quad \bar{A} = \Phi(\tau) \quad (3)$$

$$\Gamma(t) = \int_0^t e^{A(t-s)} ds B, \quad \bar{B} = \Gamma(\tau) \quad (4)$$

With these notations, the evolution of the state  $\mathbf{x}$  as a function of time can be written as

$$\begin{aligned} \mathbf{x}_k &= \bar{A}^k \mathbf{x}_0 + \sum_{i=0}^{k-1} \bar{A}^{k-i-1} \bar{B} \mathbf{r}_i \\ \mathbf{x}(t) &= \Phi(t - t_k) \mathbf{x}_k + \Gamma(t - t_k) \mathbf{r}_k, \quad \forall t \geq 0, k = \lfloor t/\tau \rfloor. \end{aligned} \quad (5)$$

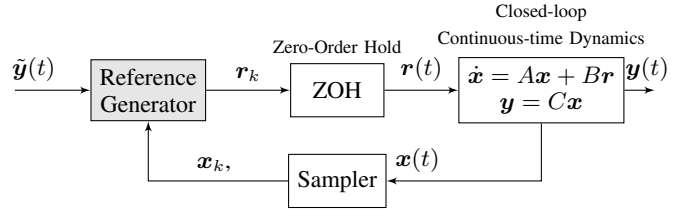


Fig. 1: Control scheme of our approach.

## III. TRAJECTORY TRACKING: THE PROBLEM

The goal of this paper is to determine the optimal references  $\mathbf{r}_k$  such that the output  $\mathbf{y}(t)$  of the system follows *as close as possible* a given target trajectory  $\tilde{\mathbf{y}}(t)$ . Figure 1 shows a blocks diagram, in which we see that:

- the inputs of our ‘‘Reference Generator’’ are:
  - the continuous-time target trajectory  $\tilde{\mathbf{y}}(t)$  and
  - the sampled state  $\mathbf{x}_k$ , while
- the output is the reference  $\mathbf{r}_k$ , which is then fed to the system after ZOH.

Let us now formally define the necessary notions and notations to properly state the problem.

- The *target trajectory* is modeled by a function  $\tilde{\mathbf{y}}(\cdot) : \mathbb{R}_+ \mapsto \mathbb{R}^p$ , which has image in the same set  $\mathbb{R}^p$  of the output  $\mathbf{y}$ . In fact, the trajectory represents a desired output to be followed, and then  $\mathbf{y}(t)$  and  $\tilde{\mathbf{y}}(t)$  must be comparable.
- The distance between the target trajectory  $\tilde{\mathbf{y}}$  and the achieved output trajectory  $\mathbf{y}$  is modeled by a weighted  $L^2$  norm, as in

$$\int_I e^{-\beta t} \|\tilde{\mathbf{y}}(t) - \mathbf{y}(t)\|^2 dt$$

with the integration interval  $I$  depending on the specific characteristics of the problem, and the weight  $e^{-\beta t}$  introduced as a discount factor to give relative importance to the near or far future. Notice that by setting  $\beta = 0$ , the norm is the standard  $L^2$  norm.

- We denote with  $t_{k'}$  the instant at which the system state  $\mathbf{x}(t_{k'})$  is sampled and a new reference  $\mathbf{r}_{k'}$  is set and held constant over the interval  $[t_{k'}, t_{k'+1})$ .
- In the following, we consider the integration interval  $[t_{k'}, t_{k'+N})$ , where  $N$  is the number of future references  $\mathbf{r}_k$  that should be computed.

Having introduced these notions, we define the optimal references  $(\mathbf{r}_{k'}, \dots, \mathbf{r}_{k'+N-1})$  as the solution that minimizes the following cost

$$\min_{(\mathbf{r}_{k'}, \dots, \mathbf{r}_{k'+N-1})} \int_{t_{k'}}^{t_{k'+N}} e^{-\beta(t-t_{k'})} \|\tilde{\mathbf{y}}(t) - \mathbf{y}(t)\|^2 dt. \quad (6)$$

## IV. TRAJECTORY TRACKING: THE SOLUTION

In this section, we develop the solution to the problem of minimizing the cost of (6). To simplify the mathematics, in this section we are going to assume that the index  $k'$  of the instant when setting the reference is equal to zero, that is,  $k' = 0$ , and that  $t_{k'} = t_0 = 0$ . At the very end of this

section and in Section V-C, we show how the proposed logic is applied in a receding horizon manner.

As in standard discretization procedures, the integral of (6) may be split over sub-intervals of length  $\tau$  so that the cost, which we label  $J$ , becomes

$$J = \int_0^{N\tau} e^{-\beta t} \|\tilde{\mathbf{y}}(t) - \mathbf{y}(t)\|^2 dt = \sum_{k=0}^{N-1} \alpha^k \int_{k\tau}^{(k+1)\tau} e^{-\beta(t-k\tau)} \|\tilde{\mathbf{y}}(t) - C\mathbf{x}(t)\|^2 dt = \sum_{k=0}^{N-1} \alpha^k \int_0^\tau e^{-\beta t} \|\tilde{\mathbf{y}}(t+k\tau) - C\Phi(t)\mathbf{x}_k - C\Gamma(t)\mathbf{r}_k\|^2 dt \quad (7)$$

with  $\alpha = e^{-\beta\tau}$ .

To proceed further, we introduce the following *inner product* between any pair of functions  $f, g : \mathbb{R} \rightarrow \mathbb{R}^p$  with image in the output space

$$\langle f, g \rangle_{\beta, \tau} = \int_0^\tau e^{-\beta t} f^\top(t)g(t) dt. \quad (8)$$

The properties of the inner product  $\langle \cdot, \cdot \rangle_{\beta, \tau}$  follow from the linearity of the integration and the properties of the scalar product over  $\mathbb{R}^p$ . Such an inner product  $\langle \cdot, \cdot \rangle_{\beta, \tau}$ , naturally induces the following norm of functions to  $\mathbb{R}^p$

$$\|f\|_{\beta, \tau} = \sqrt{\langle f, f \rangle_{\beta, \tau}} = \sqrt{\int_0^\tau e^{-\beta t} \|f(t)\|^2 dt}, \quad (9)$$

which then allows us to write more compactly the cost of (7) to be minimized, as

$$J = \sum_{k=0}^{N-1} \alpha^k \underbrace{\|\tilde{\mathbf{y}} \circ \Delta_{k\tau} - C\Phi\mathbf{x}_k - C\Gamma\mathbf{r}_k\|_{\beta, \tau}^2}_{J_k} \quad (10)$$

where  $\Delta_{k\tau}(t) = t + k\tau$  is used to denote a backward translation over time by  $k\tau$ , and  $J_k$  is used to denote more compactly the contribution to the cost  $J$  from the  $k$ -th interval. In Eq. (10), we remark that  $\tilde{\mathbf{y}} \circ \Delta_{k\tau}$ ,  $\Phi$ , and  $\Gamma$  are all functions over time, which are then integrated according to the definition of norm of (9). As in (10), we may sometimes drop the dependency on “(t)”, when using functional operators such as the inner product of (8) or the norm of (9).

In (10), we can now expand  $J_k$  by replacing  $\mathbf{x}_k$  with its explicit expression of (5) written as function of the initial state  $\mathbf{x}_0$  sampled at time 0, and all references  $\mathbf{r}_0, \dots, \mathbf{r}_{k-1}$  applied in every interval until  $k\tau$ . By doing so, we get

$$J_k = \|\tilde{\mathbf{y}} \circ \Delta_{k\tau} - C\Phi\mathbf{x}_k - C\Gamma\mathbf{r}_k\|_{\beta, \tau}^2 = \left\| \tilde{\mathbf{y}} \circ \Delta_{k\tau} - C\Phi \left( \bar{A}^k \mathbf{x}_0 + \sum_{i=0}^{k-1} \bar{A}^{k-i-1} \bar{B} \mathbf{r}_i \right) - C\Gamma\mathbf{r}_k \right\|_{\beta, \tau}^2 = \left\| \tilde{\mathbf{y}} \circ \Delta_{k\tau} - C\Phi \bar{A}^k \mathbf{x}_0 - C\Pi_k \mathbf{r} \right\|_{\beta, \tau}^2 \quad (11)$$

with:

- the vector  $\mathbf{r} \in \mathbb{R}^{mN}$  representing more compactly all the  $N$  references  $(\mathbf{r}_0, \dots, \mathbf{r}_{N-1})$  to be applied over the  $N$  control intervals, and
- the mapping  $\Pi_k : \mathbb{R} \rightarrow \mathcal{L}(\mathbb{R}^{mN}, \mathbb{R}^n)$  returning for every value of  $t$  a linear map  $\Pi_k(t) : \mathbb{R}^{mN} \rightarrow \mathbb{R}^n$ . The map  $\Pi_k(t)$  represents the impact of all the  $N$  references of  $\mathbf{r}$  onto the state  $\mathbf{x}(t)$  over the  $k$ -th interval  $[k\tau, (k+1)\tau)$ . The map  $\Pi_k$  is linear and is defined by the following matrix in  $\mathbb{R}^{n \times mN}$

$$\Pi_k = \left[ \begin{array}{cccccc} \underbrace{\text{multiply } \mathbf{r}_0}_{\Phi \bar{A}^{k-1} \bar{B}} & \dots & \underbrace{\mathbf{r}_{k-1}}_{\Phi \bar{B}} & \underbrace{\mathbf{r}_k}_{\Gamma} & \underbrace{\mathbf{r}_{k+1}}_0 & \dots & \underbrace{\mathbf{r}_{N-1}}_0 \end{array} \right] \quad (12)$$

so that

$$\Pi_k(t)\mathbf{r} = \Phi(t) \sum_{i=0}^{k-1} \bar{A}^{k-i-1} \bar{B} \mathbf{r}_i + \Gamma(t)\mathbf{r}_k.$$

The definition of each of the  $N$  blocks of  $\Pi_k$ , each one of size  $n \times m$ , reveals that:

- The block multiplying  $\mathbf{r}_k$  is set to  $\Gamma$ , which represents the impact of  $\mathbf{r}_k$  over the  $k$ -th interval itself,
- If  $i > k$ , then the  $n \times m$   $i$ -th block of  $\Pi_k$  multiplying  $\mathbf{r}_i$  is set to 0 to represent the fact that future references  $\mathbf{r}_i$  cannot have an impact on the  $k$ -th interval,
- If  $i < k$ ,  $\mathbf{r}_i$  is multiplied by  $\Phi \bar{A}^{k-i-1} \bar{B}_i$  to account for the impact of the past reference  $\mathbf{r}_i$  onto the  $k$ -th interval.

The cost  $J_k$  of (11) is quadratic in  $\mathbf{r}$ . We can then isolate each term by the degree of the dependency on  $\mathbf{r}$ . By doing so, we get

$$\begin{aligned} J_k &= \|\tilde{\mathbf{y}} \circ \Delta_{k\tau} - C\Phi \bar{A}^k \mathbf{x}_0 - C\Pi_k \mathbf{r}\|_{\beta, \tau}^2 \\ &= \|\tilde{\mathbf{y}} \circ \Delta_{k\tau} - C\Phi \bar{A}^k \mathbf{x}_0\|_{\beta, \tau}^2 && \text{(constant)} \\ &\quad - 2 \langle \tilde{\mathbf{y}} \circ \Delta_{k\tau} - C\Phi \bar{A}^k \mathbf{x}_0, C\Pi_k \mathbf{r} \rangle_{\beta, \tau} && \text{(linear)} \\ &\quad + \|C\Pi_k \mathbf{r}\|_{\beta, \tau}^2 && \text{(quadratic)} \end{aligned}$$

to isolate the constant, linear, and quadratic terms in  $\mathbf{r}$ .

The constant term  $\|\tilde{\mathbf{y}} \circ \Delta_{k\tau} - C\Phi \bar{A}^k \mathbf{x}_0\|_{\beta, \tau}^2$  has an interesting physical interpretation. It is in fact the difference between:

- the target trajectory over the  $k$ -th interval  $\tilde{\mathbf{y}} \circ \Delta_{k\tau}$ , and
- the free output evolution over the  $k$ -th interval originating from  $\mathbf{x}_0$ .

If these two functions match perfectly (i.e., the norm of their difference is zero), it is quite intuitive that there is nothing better than applying all zero references with  $\mathbf{r} = 0$ .

The inner product of the second linear term can be written as a more explicit linear function of  $\mathbf{r}$  by

$$\langle \tilde{\mathbf{y}} \circ \Delta_{k\tau} - C\Phi \bar{A}^k \mathbf{x}_0, C\Pi_k \mathbf{r} \rangle_{\beta, \tau} = \tilde{\mathbf{Y}}_k \mathbf{r} - \mathbf{x}_0^\top \mathbf{V}_k \mathbf{r}$$

with  $\tilde{\mathbf{Y}}_k \in \mathbb{R}^{1 \times mN}$  accounting for the target trajectory in the

$k$ -th interval  $[t_k, t_{k+1})$  and defined by

$$\tilde{Y}_k = [\tilde{Y}_{\Phi,k} \bar{A}^{k-1} \bar{B} \ \dots \ \tilde{Y}_{\Phi,k} \bar{B} \ \tilde{Y}_{\Gamma,k} \ 0 \ \dots \ 0] \quad (13)$$

$$\tilde{Y}_{\Phi,k} = \langle \tilde{\mathbf{y}} \circ \Delta_{k\tau}, C\Phi \rangle_{\beta,\tau} = \int_0^\tau e^{-\beta t} \tilde{\mathbf{y}}^\top(t+t_k) C\Phi(t) dt \quad (14)$$

$$\tilde{Y}_{\Gamma,k} = \langle \tilde{\mathbf{y}} \circ \Delta_{k\tau}, C\Gamma \rangle_{\beta,\tau} = \int_0^\tau e^{-\beta t} \tilde{\mathbf{y}}^\top(t+t_k) C\Gamma(t) dt \quad (15)$$

and  $\mathbf{V}_k \in \mathbb{R}^{n \times mN}$ , expressing the impact of the initial state  $\mathbf{x}_0$  over the  $k$ -th interval, defined by

$$\mathbf{V}_k = (\bar{A}^\top)^k [M_{\Phi\Phi} \bar{A}^{k-1} \bar{B} \ \dots \ M_{\Phi\Phi} \bar{B} \ M_{\Phi\Gamma} \ 0 \ \dots \ 0] \quad (16)$$

$$M_{\Phi\Phi} = \langle C\Phi, C\Phi \rangle_{\beta,\tau} = \int_0^\tau e^{-\beta t} \Phi^\top(t) C^\top C\Phi(t) dt \quad (17)$$

$$M_{\Phi\Gamma} = \langle C\Phi, C\Gamma \rangle_{\beta,\tau} = \int_0^\tau e^{-\beta t} \Phi^\top(t) C^\top C\Gamma(t) dt \quad (18)$$

Finally, the quadratic term  $\|C\Pi_k(t)\mathbf{r}\|_{\beta,\tau}^2$  of  $J_k$  is expanded as follows

$$\|C\Pi_k\mathbf{r}\|_{\beta,\tau}^2 = \langle C\Pi_k\mathbf{r}, C\Pi_k\mathbf{r} \rangle_{\beta,\tau} = \mathbf{r}^\top \mathbf{Q}_k \mathbf{r} \quad (19)$$

with  $\mathbf{Q}_k \in \mathbb{R}^{mN \times mN}$  defined by  $N \times N$  blocks of size  $m \times m$  as reported in Eq. (20) (which appears in Figure 2)

The definition of  $\mathbf{Q}_k$  in (20) exploits the definitions of  $M_{\Phi\Phi}$ ,  $M_{\Phi\Gamma}$  of Eqs. (17) and (18) respectively, and  $M_{\Gamma\Gamma}$  defined by

$$M_{\Gamma\Gamma} = \langle C\Gamma, C\Gamma \rangle_{\beta,\tau} = \int_0^\tau e^{-\beta t} \Gamma^\top(t) C^\top C\Gamma(t) dt. \quad (21)$$

The final derivation of  $\mathbf{Q}_k$  allows us to write the cost  $J_k$  accumulated in the  $k$ -th interval as

$$J_k = \|\tilde{\mathbf{y}} \circ \Delta_{k\tau} - C\Phi \bar{A}^k \mathbf{x}_0\|_{\beta,\tau}^2 - 2(\tilde{\mathbf{Y}}_k - \mathbf{x}_0^\top \mathbf{V}_k) \mathbf{r} + \mathbf{r}^\top \mathbf{Q}_k \mathbf{r}$$

and then to state the following theorem which offers the explicit expression of the cost  $J$ .

*Theorem 1:* The cost  $J$  of Equation (7) is equal to

$$J = \text{const.} - 2(\tilde{\mathbf{Y}} - \mathbf{x}_0^\top \mathbf{V}) \mathbf{r} + \mathbf{r}^\top \mathbf{Q} \mathbf{r} \quad (22)$$

with:

- $\text{const.} = \sum_{k=0}^{N-1} \alpha^k \|\tilde{\mathbf{y}} \circ \Delta_{k\tau} - C\Phi \bar{A}^k \mathbf{x}_0\|_{\beta,\tau}^2$
- $\tilde{\mathbf{Y}} = \sum_{k=0}^{N-1} \alpha^k \tilde{\mathbf{Y}}_k$

$$\mathbf{Q}_k = \begin{bmatrix} \bar{B}^\top (\bar{A}^\top)^{k-1} M_{\Phi\Phi} \bar{A}^{k-1} \bar{B} & \bar{B}^\top (\bar{A}^\top)^{k-1} M_{\Phi\Phi} \bar{A}^{k-2} \bar{B} & \dots & \bar{B}^\top (\bar{A}^\top)^{k-1} M_{\Phi\Phi} \bar{B} & \bar{B}^\top (\bar{A}^\top)^{k-1} M_{\Phi\Gamma} & 0 & \dots & 0 \\ \bar{B}^\top (\bar{A}^\top)^{k-2} M_{\Phi\Phi} \bar{A}^{k-1} \bar{B} & \bar{B}^\top (\bar{A}^\top)^{k-2} M_{\Phi\Phi} \bar{A}^{k-2} \bar{B} & \dots & \bar{B}^\top (\bar{A}^\top)^{k-2} M_{\Phi\Phi} \bar{B} & \bar{B}^\top (\bar{A}^\top)^{k-2} M_{\Phi\Gamma} & 0 & \dots & 0 \\ \vdots & \vdots & \ddots & \vdots & \vdots & \vdots & \ddots & \vdots \\ \bar{B}^\top M_{\Phi\Phi} \bar{A}^{k-1} \bar{B} & \bar{B}^\top M_{\Phi\Phi} \bar{A}^{k-2} \bar{B} & \dots & \bar{B}^\top M_{\Phi\Phi} \bar{B} & \bar{B}^\top M_{\Phi\Gamma} & 0 & \dots & 0 \\ M_{\Phi\Gamma}^\top \bar{A}^{k-1} \bar{B} & M_{\Phi\Gamma}^\top \bar{A}^{k-2} \bar{B} & \dots & M_{\Phi\Gamma}^\top \bar{B} & M_{\Gamma\Gamma} & 0 & \dots & 0 \\ 0 & 0 & \dots & 0 & 0 & 0 & \dots & 0 \\ \vdots & \vdots & \ddots & \vdots & \vdots & \vdots & \ddots & \vdots \\ 0 & 0 & \dots & 0 & 0 & 0 & \dots & 0 \end{bmatrix} \quad (20)$$

Fig. 2: Expression of  $\mathbf{Q}_k$

- $\mathbf{V} = \sum_{k=0}^{N-1} \alpha^k \mathbf{V}_k$
- $\mathbf{Q} = \sum_{k=0}^{N-1} \alpha^k \mathbf{Q}_k$

*Proof:* The proof is constructed by the steps preceding the theorem statement. ■

Theorem 1 states that the cost, as initially defined by (7) is a quadratic form in  $\mathbf{r}$ . The determination of the optimal  $\mathbf{r}$  that minimizes such a cost, however, depends on the characteristics of the linear and the quadratic terms of (22). Next, we offer a couple of technical lemmas, which makes another step for determining the optimal solution.

*Lemma 1:* The matrix  $\mathbf{Q} \in \mathbb{R}^{mN \times mN}$  is:

- symmetric, and
- positive semi-definite.

*Proof:* From the definitions of Eqs. (17) and (21) the square matrices  $M_{\Phi\Phi}$  and  $M_{\Gamma\Gamma}$  are symmetric and then from the definition of Eq. (20),  $\forall k$  the matrices  $\mathbf{Q}_k$  are symmetric too.  $\mathbf{Q}$  is a linear combination of matrices  $\mathbf{Q}_k$ , so it is symmetric.

From (19) it follows that  $\forall \mathbf{r}, \mathbf{r}^\top \mathbf{Q}_k \mathbf{r} \geq 0$  because it is equal to  $\|C\Pi_k\mathbf{r}\|_{\beta,\tau}^2$  which is the square of a norm. Hence,  $\forall k$  the matrix  $\mathbf{Q}_k$  is positive semi-definite. Since  $\mathbf{Q}$  is a linear combination of matrices  $\mathbf{Q}_k$  with non-negative coefficients  $\alpha^k$ , then  $\mathbf{Q}$  is also positive semi-definite. This concludes the proof. ■

The matrix  $\mathbf{Q}$  is then positive semi-definite. It may, however, not be strictly positive definite. The next lemma provides some insights about the null space of  $\mathbf{Q}$  so that we can find the minimum of the cost of (22).

*Lemma 2:* If  $\mathbf{r} \in \ker \mathbf{Q}$  then  $\mathbf{r} \in \ker(\tilde{\mathbf{Y}} - \mathbf{x}_0^\top \mathbf{V})$ .

*Proof:* We prove the statement by contradiction. Let us assume to have some  $\mathbf{r}^*$  such that  $\mathbf{r}^* \in \ker \mathbf{Q}$  and  $\mathbf{r}^* \notin \ker(\tilde{\mathbf{Y}} - \mathbf{x}_0^\top \mathbf{V})$ . Obviously it must be  $\mathbf{r}^* \neq 0$ . For such a choice of references  $\mathbf{r}^*$ , the corresponding cost  $J$  of (22) is

$$\begin{aligned} J(\mathbf{r}^*) &= \text{const.} - 2(\tilde{\mathbf{Y}} - \mathbf{x}_0^\top \mathbf{V}) \mathbf{r}^* + (\mathbf{r}^*)^\top \mathbf{Q} \mathbf{r}^* \\ &= \text{const.} - 2(\tilde{\mathbf{Y}} - \mathbf{x}_0^\top \mathbf{V}) \mathbf{r}^* \end{aligned}$$

If  $(\tilde{\mathbf{Y}} - \mathbf{x}_0^\top \mathbf{V}) \mathbf{r}^* > 0$  then it is possible to find a large enough  $\lambda > 0$  such that  $J(\lambda \mathbf{r}^*) < 0$ . This, however, is not possible because it is always  $J \geq 0$ . An analogous argument can be used if  $(\tilde{\mathbf{Y}} - \mathbf{x}_0^\top \mathbf{V}) \mathbf{r}^* < 0$ . This leads to a contradiction. Then it must be  $\mathbf{r}^* \in \ker(\tilde{\mathbf{Y}} - \mathbf{x}_0^\top \mathbf{V})$ , as required. ■

Lemma 1 states that  $\mathbf{Q}$  is positive semi-definite and symmetric. Hence it can be diagonalized as follows:

$$\begin{bmatrix} \Lambda & 0 \\ 0 & 0 \end{bmatrix} = \begin{bmatrix} H^\top \\ H_0^\top \end{bmatrix} \mathbf{Q} \begin{bmatrix} H & H_0 \end{bmatrix}$$

with:

- $\Lambda$  the diagonal matrix with the strictly positive eigenvalue of  $\mathbf{Q}$ ,
- $\begin{bmatrix} H & H_0 \end{bmatrix}$  the orthonormal matrix which diagonalizes  $\mathbf{Q}$ ,
- the columns of  $H_0$  are an orthonormal basis of  $\ker \mathbf{Q}$ , and
- the columns of  $H$  are an orthonormal basis of the subspace of  $\mathbb{R}^{mN}$  orthogonal to  $\ker \mathbf{Q}$ .

From Lemma 2, any vector in  $\ker \mathbf{Q} = \text{span } H_0$  also belongs to the null-space of  $(\tilde{\mathbf{Y}} - \mathbf{x}_0^\top \mathbf{V})$ . Hence, the space of all solutions is

$$\{\mathbf{r}^*\} + \text{span } H_0 = \{\mathbf{r}^* + \mathbf{v} : \mathbf{v} \in \text{span } H_0\} \quad (23)$$

with  $\mathbf{r}^* = H\mu$ , for some linear combination  $\mu$  of the basis  $H$ , found by the following standard minimization of a quadratic form

$$\begin{aligned} J &= \text{const.} - 2(\tilde{\mathbf{Y}} - \mathbf{x}_0^\top \mathbf{V})H\mu + \mu^\top H^\top \mathbf{Q}H\mu \\ J &= \text{const.} - 2(\tilde{\mathbf{Y}} - \mathbf{x}_0^\top \mathbf{V})H\mu + \mu^\top \Lambda \mu \\ \nabla J &= -2(\tilde{\mathbf{Y}} - \mathbf{x}_0^\top \mathbf{V})H + 2\mu^\top \Lambda \end{aligned}$$

and by setting the gradient equal to zero

$$\begin{aligned} -2(\tilde{\mathbf{Y}} - \mathbf{x}_0^\top \mathbf{V})H + 2\mu^\top \Lambda &= 0 \\ \mu^\top \Lambda &= (\tilde{\mathbf{Y}} - \mathbf{x}_0^\top \mathbf{V})H \\ \Lambda \mu &= H^\top (\tilde{\mathbf{Y}}^\top - \mathbf{V}^\top \mathbf{x}_0) \\ \mu &= \Lambda^{-1} H^\top (\tilde{\mathbf{Y}}^\top - \mathbf{V}^\top \mathbf{x}_0) \\ \mathbf{r}^* &= H \Lambda^{-1} H^\top (\tilde{\mathbf{Y}}^\top - \mathbf{V}^\top \mathbf{x}_0). \end{aligned} \quad (24)$$

This allows us to conclude that all solutions that minimize the cost of (7) belong to  $\{\mathbf{r}^*\} + \text{span } H_0$ , with  $\mathbf{r}^*$  from (24). Which solution to pick in this set may respond to different goals, such as robustness. This further investigation, however, is left as future work.

Any given solution  $\mathbf{r}^*$  is, we remind, the collection  $(\mathbf{r}_0^*, \mathbf{r}_1^*, \dots, \mathbf{r}_{N-1}^*)$  of all the  $N$  references to be applied over the next  $N$  intervals to achieve minimal cost. References, however, are computed in closed-loop upon the state is sampled. Hence, they can be applied in a receding horizon manner:

- only  $\mathbf{r}_0^*$  is applied over  $[t_0, t_1)$
- at  $t_1$  a new state  $\mathbf{x}_1$  is sampled, possibly different than the ideal state evolution  $\bar{A}\mathbf{x}_0 + \bar{B}\mathbf{r}_0^*$ , because of noise or model inaccuracies, and based on it a new optimal reference is computed and applied over  $[t_1, t_2)$ .

Clearly, the computation of the new reference value can take advantage of past computation due to the similarity of the expressions. The numerical optimization of this procedure will be investigated in the future. Note that, due to the form of  $\bar{A}$ , if the closed-loop continuous-time matrix  $A$  is not

asymptotically stable, possible numerical issues may arise in the solution of the optimization procedure.

This receding horizon approach is explored in Section V-C through a mobile robotics use case in which optimal waypoints are used to control the motion of an unmanned aerial vehicle.

## V. SIMULATIONS

The simulation code and the corresponding videos of the results described in this section can be accessed through the public repository available at [https://github.com/ebni/opt\\_ref\\_track](https://github.com/ebni/opt_ref_track).

### A. Impact of $\beta$

In this section, we briefly explore the impact of  $\beta$ . As shown in Equation (6):

- if  $\beta = 0$  then the differences between the target trajectory  $\tilde{\mathbf{y}}(t)$  and the output  $\mathbf{y}(t)$  are all equally accounted in the integral of the cost,
- if  $\beta < 0$  then the difference is weighted more for later time instants, while
- if  $\beta > 0$ , the difference between the target and the output is weighted more at earlier times.

We evaluate the impact of  $\beta$  on a simple double integrator controlled by a PD, which has the following closed-loop matrices

$$A = \begin{bmatrix} 0 & 1 \\ -K_P & -K_D \end{bmatrix}, B = \begin{bmatrix} 0 \\ K_P \end{bmatrix}. \quad (25)$$

In this simulation, the gains of the internal controller were set as  $K_P = 2$  and  $K_D = 3$ .

The initial system state is  $\mathbf{x}(0) = [0 \ 0]^T$ , which also corresponds to a zero output  $\mathbf{y}(0) = 0$ .

In the first example, we find the optimal references  $\{\mathbf{r}_k\}$  so that the output follows as close as possible the target trajectory

$$\tilde{\mathbf{y}}(t) = \left( \frac{1 - \cos(2\pi t)}{2} \right)^8. \quad (26)$$

Such a trajectory is chosen because starting from zero, it requires to quickly reach 1 at time  $t = 0.5$ , and then go back to zero.

Figure 3 shows the achieved output  $\mathbf{y}(t)$  and the corresponding optimal references  $\{\mathbf{r}_k\}$  minimizing the cost of Eq. (6). The three plots correspond to three different values of  $\beta \in \{-10, 0, 10\}$ . We observe that for  $\beta = 10$  the trajectory is more tightly followed before reaching the peak at time  $t = 0.5$ . Also, we observe that, given the symmetry of the target trajectory w.r.t. time  $t = 0.5$ , the achieved output when  $\beta = -10$  is the ‘‘mirror’’ of the output when  $\beta = 10$ .

The second example has the very same settings as above, with the only difference of the target trajectory  $\tilde{\mathbf{y}}(t)$ , which is set equal to the unit step occurring at  $t = 0$  as follows

$$\tilde{\mathbf{y}}(t) = \text{step}(t) = \begin{cases} 1 & t > 0 \\ 0 & t \leq 0. \end{cases} \quad (27)$$

The output and optimal references are reported in Figure 4 for the same values of  $\beta \in \{-10, 0, 10\}$  as above. We notice

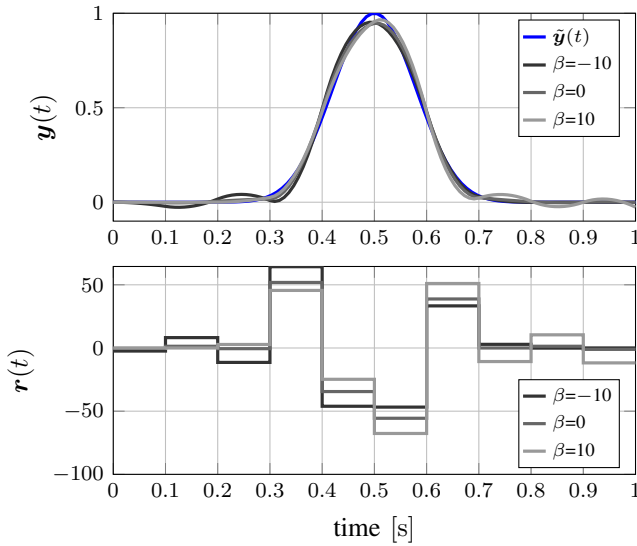


Fig. 3: Top: target trajectory  $\tilde{y}(t)$  (blue) and achieved output  $y(t)$  for different choices of  $\beta$  (grays). Bottom: optimal sequence of references.

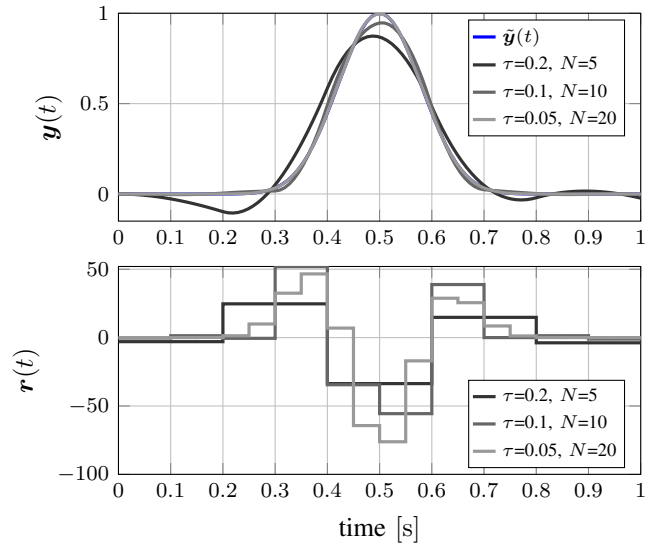


Fig. 5: Top: target trajectory  $\tilde{y}(t)$  (blue) and achieved output  $y(t)$  for different choices of  $\tau$  and  $N$  (grays). Bottom: optimal sequence of references.

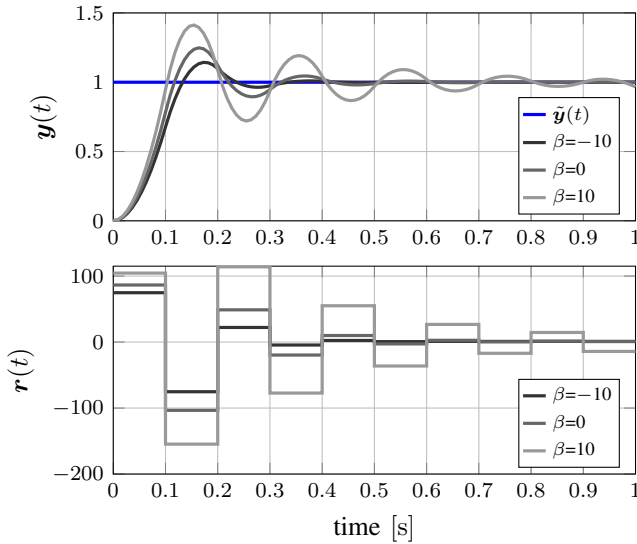


Fig. 4: Top: target trajectory  $\tilde{y}(t) = \text{step}(t)$  (blue) and achieved output  $y(t)$  for different choices of  $\beta$  (grays). Bottom: optimal sequence of references.

that a choice of negative  $\beta$  achieves a better asymptotic behavior. On the other hand, if a more rapid converge to the desired set point is desired, then a positive  $\beta$  should be preferred.

### B. Impact of sampling period

In this section, we explore the impact of the period  $\tau$  for which each single reference is held. We borrow the PD-controlled double integrator with closed loop matrices  $A$  and  $B$  as in Equation (25). Also, in this section we assume  $\beta = 0$  meaning that we give equal weight over time to the distance between  $\tilde{y}(t)$  and  $y(t)$ , as indicated in the cost of Eq. (6).

The simulation of Figure 5 shows the evolution of the output when the trajectory  $\tilde{y}(t)$  to be tracked is the same of Equation (26). The three plots correspond to three different values of the holding time  $\tau \in \{0.04, 0.1, 0.2\}$  and the number of intervals  $N \in \{25, 10, 5\}$ . Not surprisingly, we observe that the smaller is  $\tau$  the closer the output  $y(t)$  is to the target  $\tilde{y}(t)$ . Another phenomenon worth commenting on is that when  $\tau = 0.2$  and  $N = 5$ , the optimal references need to anticipate (at time  $t = 0.2$ ) the coming growth of the target trajectory, otherwise it may be too late (and too costly according to (6)) to react at  $t = 0.4$ .

The simulation of Figure 6 shows, with the same values of  $\tau$  and  $N$  of Figure 5, the output when the target trajectory is a step. The main comment worth making is that in response to the discontinuity of the target at the origin, the first reference  $r_0$  is always very large. Moreover, such a value grows as the interval  $\tau$  decreases.

### C. The UAV use case

For real-world systems, it is common to define an optimal control problem over a fixed prediction time horizon and continually find solutions by receding this horizon as the system evolves. This is done to compensate for model inaccuracies or random disturbances, as well as find a computationally tractable approximation of the infinite-time horizon control problem. In order to validate the proposed solution in a realistic situation, the optimal control problem defined in Eq. (6) was continually solved in a receding horizon fashion for a linearized two-dimensional unmanned aerial vehicle (UAV) system. Depending on the orientation of the UAV, the motors can provide forces in a 2D plane. When linearized about hovering, the UAV acts as two decoupled double integrator systems, acting independently in each direction. Thus, it is possible to use the closed-loop matrices  $A$  and  $B$

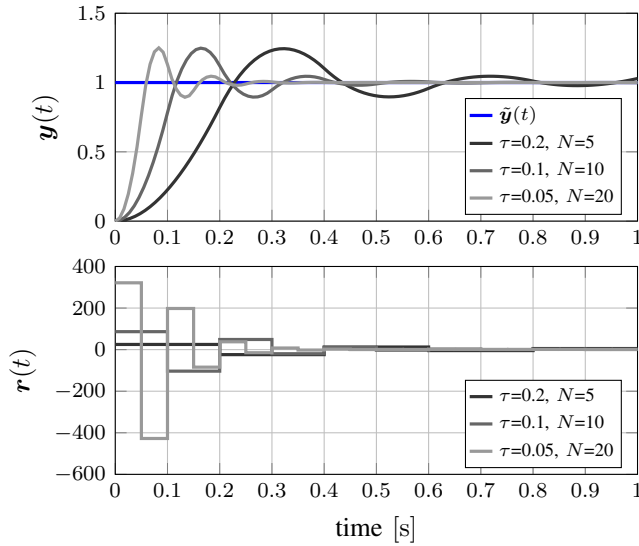


Fig. 6: Top: target trajectory  $\tilde{\mathbf{y}}(t) = \text{step}(t)$  (blue) and achieved output  $\mathbf{y}(t)$  for different choices of  $\tau$  and  $N$  (grays). Bottom: optimal sequence of references.

of Eq. (25) as a means of modeling motion over the plane. In this case, the internal state  $\mathbf{x}(t) \in \mathbb{R}^4$  contains position and velocity of both coordinates over the plane, and the control input  $\mathbf{u}(t)$  represents forces in the plane that map to motor speeds of the UAV.

Additionally, it is common to define waypoints in the plane for the UAV to move towards. In the context of this work, the waypoint is a reference  $\mathbf{r}_k$  for the system to track over time interval  $[t_k, t_k + \tau)$ , and such tracking is done by a PD controller.

The optimal reference signal was tasked with commanding the UAV to track the following target trajectory:

$$\tilde{\mathbf{y}}(t) = \begin{bmatrix} 4 \sin(t) \\ 2 \sin(2t) \end{bmatrix}. \quad (28)$$

Fig. 7 shows the resulting motion of the UAV for different values of the holding time  $\tau = \{0.1, 0.25, 0.5\}$ . In order to make a fair comparison, the number of prediction intervals  $N$  was also modified so that the total prediction horizon was defined over 2 seconds into the future. Initially, at  $t = 0$ , the optimal waypoints were computed for the next 2 seconds. The first optimal waypoint  $\mathbf{r}_1$  was applied to the system, and after  $\tau$  time, another set of optimal waypoints was found over  $t = [\tau, \tau + 2]$ . This process was repeated in a receding horizon fashion, with Fig. 7 also showing the receding horizon (RH – dashed line in the figure) at time  $t = 3.0$ . Included is the norm of the difference between the target trajectory and the actual trajectory over time, i.e.,  $\|\tilde{\mathbf{y}}(t) - \mathbf{y}(t)\|$ , for each choice  $\tau$ .

When  $\tau = 0.1$ s,  $N = 20$  optimal waypoints were found that could track the target trajectory with small difference. With  $\tau = 0.25$ s, only  $N = 8$  optimal waypoints were chosen over the 2s receding horizon, resulting in a larger difference. Worse still was  $\tau = 0.5$ s with  $N = 4$  optimal waypoints.

Intuitively, this reflects the notion that a faster sampling rate results in better tracking of the target trajectory.

## VI. CONCLUSION AND FUTURE WORK

This paper presented an approach to optimally compute the discrete-time reference signal  $\mathbf{r}_k$  given a desired continuous-time trajectory  $\tilde{\mathbf{y}}(t)$  that the system output  $\mathbf{y}(t)$  should follow. The presented approach was presented for the case of periodic sampling and has investigated its effects on the obtainable performance over different examples, including a UAV use case.

Future works will be devoted to the investigation of the impact of limited processing and communication capacity on the quality of the achieved control. Directions of investigation include the exploration of non-periodic sampling, the evaluation of the impact of quantization, and the exploitation of past computations when calculating references in a receding horizon fashion.

Finally, we plan to apply the presented approach to additional use case applications, including experimental results in our evaluation, and further investigate its robustness against model uncertainty.

## REFERENCES

- [1] S. Schneider, A. Bylard, T. G. Chen, P. Wang, M. Cutkosky, M. Lapôtre, and M. Pavone, “Reachbot: A small robot for large mobile manipulation tasks,” in *2022 IEEE Aerospace Conference (AERO)*. IEEE, 2022, pp. 1–12.
- [2] K. Chu, M. Lee, and M. Sunwoo, “Local path planning for off-road autonomous driving with avoidance of static obstacles,” *IEEE Transactions on Intelligent Transportation Systems*, vol. 13, no. 4, pp. 1599–1616, 2012.
- [3] J. Han, D. Kim, M. Lee, and M. Sunwoo, “Enhanced road boundary and obstacle detection using a downward-looking lidar sensor,” *IEEE Transactions on Vehicular Technology*, vol. 61, no. 3, pp. 971–985, 2012.
- [4] J. Ragazzini and G. Franklin, *Sampled-data Control Systems*. New York, NY: McGraw-Hill, 1958.
- [5] T. Chen and B. Francis, *Optimal Sampled-Data Control Systems*, ser. Communications and Control Engineering. Springer London, 2012.
- [6] R. Alur, D. Hristu-Varsakelis, K. Årzén, W. Levine, J. Baillieul, and T. Henzinger, *Handbook of Networked and Embedded Control Systems*, ser. Control Engineering. Birkhäuser Boston, 2007.
- [7] M. Seron, J. Braslavsky, and G. Goodwin, *Fundamental Limitations in Filtering and Control*, ser. Communications and Control Engineering. Springer London, 2012.
- [8] S. Hara, H. Fujioka, and P. T. Kabamba, “A hybrid state-space approach to sampled-data feedback control,” *Linear Algebra and its Applications*, vol. 205-206, pp. 675–712, Jul. 1994.
- [9] J. C. Geromel, P. Colaneri, and P. Bolzern, “Differential linear matrix inequality in optimal sampled-data control,” *Automatica*, vol. 100, pp. 289–298, 2019.
- [10] T. Chen and B. A. Francis, *Optimal Sampled-Data Control Systems*. London, UK: Springer-Verlag, 1995.
- [11] S. Boyd, L. El Ghaoui, E. Feron, and V. Balakrishnan, *Linear matrix inequalities in system and control theory*. Philadelphia, PA: SIAM, 1994.
- [12] J. C. Geromel and M. Souza, “On an LMI approach to optimal sampled-data state feedback control design,” *International Journal of Control*, vol. 88, no. 11, pp. 2369–2379, 2015.
- [13] J.-H. Hwang, R. Arkin, and D.-S. Kwon, “Mobile robots at your fingertip: Bezier curve on-line trajectory generation for supervisory control,” in *IEEE/RSJ International Conference on Intelligent Robots and Systems (IROS)*, vol. 2, 2003, pp. 1444–1449 vol.2.
- [14] S. Liu and D. Sun, “Minimizing energy consumption of wheeled mobile robots via optimal motion planning,” *IEEE/ASME Transactions on Mechatronics*, vol. 19, no. 2, pp. 401–411, 2014.

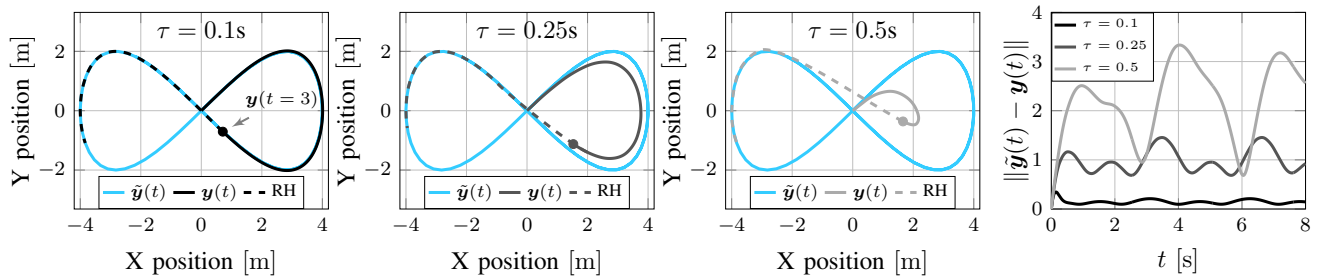


Fig. 7: Simulation showing a UAV use case in which optimal waypoints are computed in a receding horizon fashion. Also included is the difference between the actual trajectory and the target trajectory over time.

- [15] C. Hildebrandt, S. Elbaum, N. Bezzo, and M. B. Dwyer, “Feasible and stressful trajectory generation for mobile robots,” in *Proceedings of the 29th ACM SIGSOFT International Symposium on Software Testing and Analysis*, ser. ISSTA 2020. New York, NY, USA: Association for Computing Machinery, 2020, p. 349362.
- [16] R. Penicka and D. Scaramuzza, “Minimum-time quadrotor waypoint flight in cluttered environments,” *IEEE Robotics and Automation Letters*, pp. 1–1, 2022.
- [17] B. Lau, C. Sprunk, and W. Burgard, “Kinodynamic motion planning for mobile robots using splines,” in *IEEE/RSJ International Conference on Intelligent Robots and Systems (IROS)*, 2009, pp. 2427–2433.
- [18] D. Mellinger and V. Kumar, “Minimum snap trajectory generation and control for quadrotors,” in *2011 IEEE international conference on robotics and automation*. IEEE, 2011, pp. 2520–2525.
- [19] Z. Wang, X. Zhou, C. Xu, J. Chu, and F. Gao, “Alternating minimization based trajectory generation for quadrotor aggressive flight,” *IEEE Robotics and Automation Letters*, vol. 5, no. 3, pp. 4836–4843, 2020.
- [20] Y. Yang, P. Long, X. Song, J. Pan, and L. Zhang, “Optimization-based framework for excavation trajectory generation,” *IEEE Robotics and Automation Letters*, vol. 6, no. 2, pp. 1479–1486, 2021.
- [21] J. Higgins, E. Bini, and N. Bezzo, “Offloaded receding horizon planning for environments with variable communication delays,” in *Proceedings of the 6th IEEE Conference on Control Technology and Applications (CCTA)*, Trieste, Italy, 2022.